Chemistry–A European Journal
Research Article
doi.org/10.1002/chem.202202407
Chemistry Europe
European Chemical Societies Publishing
www.chemeurj.org

Borate Buffer as a Key Player in Cu-Based Homogeneous Electrocatalytic Water Oxidation

Guilin Ruan,[a] Natalia Fridman,[a] and Galia Maayan*[a]

Abstract: Borate buffer was found to have both structural and functional roles within a low-cost tri-copper electrocatalyst for homogeneous water oxidation that exhibits a high turnover frequency of 310 s^{-1}. The borate buffer was shown to facilitate the catalytic activity by both bridging the three Cu ions and participating in O–O bond formation. Phosphate and acetate buffers did not show such roles, making borate a unique player in this catalytic system.

Introduction

Water electrolysis is a promising approach for producing hydrogen fuel as renewable energy,[1] however, the high overpotential and slow kinetics of water oxidation (WO) limit its applicability.[2] An important task is therefore to understand the role of each component in WO systems, including the one of the buffer.[3] In the past decade, Cu-based molecular WO electrocatalysts showed high potential due to the significantly fast kinetics of Cu^{II}-2,2′-bipyridine (Cu^{II}(BPy)) systems.[4] Also, even without a ligand system, some Cu salts can perform as WO electrocatalysts in specific buffer solutions,[5] with high stability and excellent homogeneity. However, Cu^{II}(BPy) systems require high overpotential and/or high pH conditions,[4] while naked Cu salts are not efficient, resulting in only low turnover frequency (TOF) values.[6]

Although the choice of a buffer can play a crucial role in the catalytic activity during WO, the role of the buffer species, in contrast to the roles of the metal ion(s) and supporting ligand(s), is rarely explored.[7] To date, the most common solutions used for WO studies are the commercially available and low-cost: acetate, phosphate, and borate buffers. Typically, the choice of a buffer depends on the desired pH conditions rather than on its role in the catalytic process (catalyst design). However, in phosphate buffer at pH 7.0, Co ions are found to form in situ Co-phosphate film on the working electrode that performs as a heterogeneous electrocatalyst for WO.[8] Likewise, both Ni and Cu ions can form an in situ active layer on an electrode in borate buffer at a pH of about 9.[9] These studies indicate the significance of the interactions between buffer environments and metal ions during WO, but the fundamental understanding of these interactions is still limited. Lately, two studies suggest that the borate anion $B(OH)_4^-$ can act as a cocatalyst for Cu-catalyzed WO, by acting as a carrier of an oxygen atom that participates in the O–O bond formation step.[5c][10] The cooperativity between the borate buffer and the Cu complexes appreciably leads to high TOF at a pH of about 9.[10]

To better understand the superiority of borate buffer over other solution media in Cu-based homogeneous electrocatalytic WO, and quantify its contribution for the first time, we intended to design a unique Cu-borate complex and investigate its electrocatalytic properties towards WO. Such a design may assist in discovering other unexplored roles of borate species, as well as motivate the future design of Cu-based oxidation catalysis with borate. To this aim, we chose to use the simple, low-cost, soluble, and stable complex, $[Cu(BPy)_2(ClO_4)]^+$ in different buffers including borate.[11] During our studies, we have discovered that when dissolved in 0.2 M borate buffer at pH 9, three $[Cu(BPy)_2(ClO_4)]^+$ cations can form an in situ trinuclear complex, $\{[Cu(BPy)_2]_3B(O)_3\}^{3+}$ (CuBor, Figure 1), with a BO_3^{3-} borate anion as a central bridge, which is a novel structural role of the borate buffer. Moreover, CuBor was found to be a stable and efficient WO electrocatalyst, compared with the electrochemical properties of $[Cu(BPy)_2(ClO_4)]^+$ in other buffer solutions (phosphate and acetate) and other reported

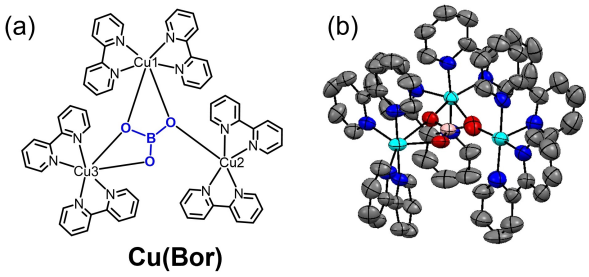

Figure 1. (a) molecular structure and (b) ORTEP view of CuBor crystalized from borate buffer at pH 9. The guest molecules (perchlorate and water) in the crystal structure are omitted for clarity.

[a] G. Ruan, N. Fridman, Prof. G. Maayan
Schulich Faculty of Chemistry
Technion-Israel Institute of Technology
Technion City, Haifa 3200008 (Israel)
E-mail: gm92@technion.ac.il

Supporting information for this article is available on the WWW under https://doi.org/10.1002/chem.202202407

Cu^{II}(BPy)-based derivatives (Table S1). Notably, CuBor can oxidize water sustainably to dioxygen for at least 10 h during control potential electrolysis (CPE) with high Faradaic efficiency (FE%) of 91%. We further discovered that the borate buffer exclusively enhances the kinetic properties of CuBor with a considerable turnover frequency (TOF_0) parameter of 310 s^{-1}, as calculated by foot-of-the-wave analysis (FOWA).[12] In addition, the buffer-dependent rate constant k_B was calculated to be 7.5×10^2 M^{-1} s^{-1}, which is considerably high as compared to reported values of other buffers (see Table S2 for references).

Results and Discussion

$[Cu(BPy)_2(ClO_4)]^+$ was easily prepared by modifying a previously reported procedure[11] using $Cu(ClO_4)_2\bullet6H_2O$ instead of $Cu(NO_3)_2$, as perchlorate plausibly assists in the crystallization of the Cu complexes.[13] Its molecular structure was confirmed by crystallization from water (Figure S1&S34). We then redissolved $[Cu(BPy)_2(ClO_4)]^+$ crystal in borate buffer at pH 9, which is below the pKa of boric acid (9.2),[14] and obtained a completely different structure: a new in situ molecule was generated, in which a BO_3^{3-} anion bridges three units of $[Cu(BPy)_2(ClO_4)]^+$, forming a trinuclear structure, CuBor, as shown in Figures 1 and S33. In this new trinuclear complex, only Cu2 coordinates to four N atoms from two 2,2′-bipyridine ligands and one O atom from BO_3^{3-} bridge, exhibiting penta-coordination leaving a free coordination site for potential binding of a guest molecule or a substrate (e.g., H_2O). The two other Cu centres, Cu1 and Cu3, are hexa-coordinated to four N atoms of the two bipyridine ligands and to two O atoms from BO_3^{3-} but they are not identical as evident from the differences between the bond lengths and angles within each Cu center (Table S4&S5). Bond valence sum (BVS) calculations are obtained as 2.21, 2.14, and 2.05 for Cu1, Cu2, and Cu3, respectively, based on the determined Cu–N and Cu–O distances from the X-ray structure (Eq. S1-2, Table S10), indicating that three Cu centres are all in Cu^{II} oxidation state.[15]

The UV-Vis spectrum of CuBor in water revealed absorption bands near 234, 288, 298, 310, and 660 nm that are all linearly dependent on its concentration (Figure S2). In comparison, the UV-Vis spectrum of $[Cu(BPy)_2(ClO_4)]^+$ includes bands near 239, 299, 310, and 743 nm, lacking the absorption band at 288 nm ($\varepsilon = 20616$ M^{-1} cm^{-1}, Figure S3). These differences suggest that CuBor exists in solution phase as single species instead of decomposing to be $[Cu(BPy)_2(ClO_4)]^+$ (Figure S4). The absorption band near 288 nm, which can be assigned to the interaction between Cu and borate, is also obtained when $[Cu(BPy)_2(ClO_4)]^+$ is dissolved in borate buffer pH 9, suggesting the kinetic formation of CuBor in solution (Figure S5).[5c][10] Notably, below or above pH 9, the absorbance intensity near 288 nm decreased, indicating that the formation of CuBor is pH-dependent and that CuBor is the most stable at pH 9. Moreover, when a sample of the CuBor crystal was re-dissolved in borate buffer at pH 9, the same spectrum was obtained and it remained identical after 24 h, indicating that CuBor is also thermodynamically stable (Figure S6). The existence of CuBor in solution was further evidenced by Attenuated total reflectance - Fourier-transform infrared spectroscopy (ATR-FTIR) Electron paramagnetic resonance (EPR). The ATR-FTIR analysis of CuBor in borate buffer at pH 9 showed a discernible transmittance at 868 cm^{-1}. A similar band at this range was not obtained when analyzing $Cu(BPy)_2(ClO_4)]^+$ in water (Figure S7) and therefore the band at 868 cm^{-1} was assigned to the BO^{3-} bridge in a sample of CuBor in borate buffer.[16] The EPR spectra of CuBor in borate buffer at pH 9 showed a board signal ($g = 4.23$) in half-field region (Figure S8), which is in accordance with the relevant literature.[16b][17] The intensity of the signal decreased at pH 11 ($g = 4.18$) and dissapeared at pH 7, indicating that the weak interactions among multinuclear Cu(II) ions exist at pH 9 and 11 (weaker) but disappear at pH 7. Indeed, crystal of the mononuclear precursor $[Cu(BPy)_2(ClO_4)]^+$ was obtained from borate buffer at pH 7.

Cyclic voltammetry (CV) scans of CuBor and that of $[Cu(BPy)_2(ClO_4)]^+$ were performed in 0.2 M borate buffer at pH 9. The results show identical oxidative activity (Figure 2a&2d, Figure S9), in accordance to the results obtained from the UV-Vis measurements of CuBor and $[Cu(BPy)_2(ClO_4)]^+$ under the same conditions. However, when $[Cu(BPy)_2(ClO_4)]^+$ was dissolved in phosphate buffer, only one oxidation peak, with low current intensity, was observed (Figure 2b). Similarly, negligible oxidation was obtained in acetate buffer (Figure 2c). Indeed, $[Cu(BPy)_2(ClO_4)]^+$ dissolved in phosphate and acetate buffers at pH 9.0 resulted in different structures, which were also different from the structure obtained in borate buffer, as determined by

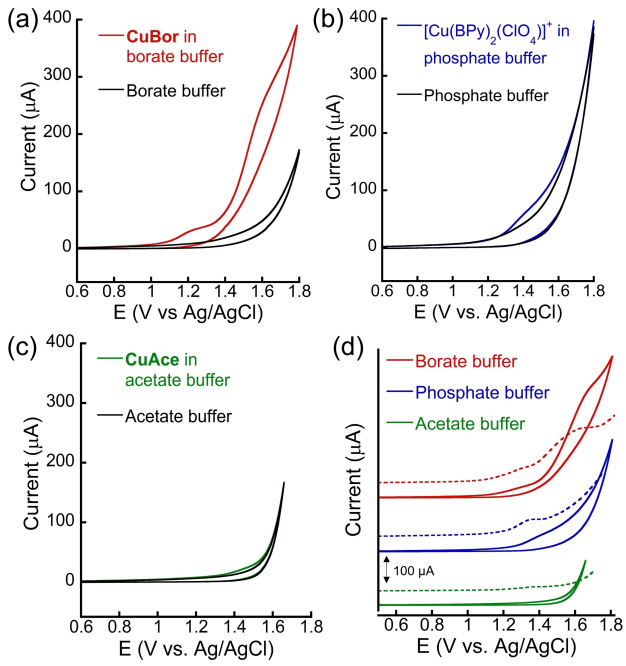

Figure 2. CVs with and without 0.5 mM (a) CuBor, (b) $[Cu(BPy)_2(ClO_4)]^+$, and (c) CuAce in 0.2 M borate, phosphate, and acetate buffer solutions at pH 9, respectively, at scan rate 50 mV/s; (d) CVs (solid) and DPVs (dashed) of 1.5 mM $[Cu(BPy)_2(ClO_4)]^+$ in 0.2 M borate buffer and 0.5 mM in other 0.2 M buffer solutions at pH 9, at scan rate 50 mV/s. All the measurements were done with glassy carbon as working electrode (0.07 cm^2), Ag/AgCl as reference electrode.

X-ray crystallography. In phosphate buffer, the structure of $[Cu(BPy)_2(ClO_4)]^+$ was identical to its structure obtained from water, while in acetate buffer, two coordinated ClO_4^- were replaced by one OAc^- as bidentate ligand, $[Cu(BPy)_2(OAc)]^+$, (CuAce, Figures S1 & S35).[18] These observations strongly indicate that the oxidation of CuAce in acetate buffer is prohibited by the chelation of OAc^-, whereas the oxidative activity of CuBor is contributed by the unique skeleton of BO_3^{3-} bridge versus its pre-complex $[Cu(BPy)_2(ClO_4)]^+$ in phosphate buffer.

To further test whether CuBor is stable and catalytically active in other buffer solutions, the crystal of CuBor was re-dissolved in acetate and in phosphate buffers at pH 9. The UV-Vis spectrum of these solutions showed an absorbance band near 288 nm albeit with lower intensity compared to that in borate buffer (Figure S10). However, the CV in these solutions did not exhibit a significant current enhancement as in borate buffer. These control experiments indicate that CuBor is not only most stable in borate buffer, but more importantly, that borate buffer is required for the electrocatalytic activity of CuBor towards WO.

The electrochemical properties of CuBor were therefore further investigated in 0.2 M borate buffer at pH 9.0. The CV of CuBor measured in these conditions showed two irreversible shoulder waves at +1.25 V and +1.55 V, respectively, which were determined more clearly in differential pulse voltammetry (DPV, Figure 2d). To understand how many electrons are transferred in the first oxidation event, the plot of $E_{p/2}$ vs. ln(υ) was fitted by Laviron equation.[19] The linear slope of this anodic reaction is equal to RT/(1-α)nF, where n (the number of electron transfer) is calculated as 2 (Eq. S3–4, Figure S11). Hence, two electrons are transferred in this event. As in previous studies of Cu^{II}-BPy system,[4] Cu^{II} is superiorly oxidized over BPy ligand, unless any redox-active group (e.g., phenolic) is coordinated. Therefore, this oxidation event is assigned to the oxidation of Cu^{II} to Cu^{III} in two Cu centers. This assignment may illustrate the benefits of the BO_3^{2-} bridge, which assembles a trinuclear structure and assists with electron transfer. The comparison of CuBor in borate buffer and $[Cu(BPy)_2(ClO_4)]^+$ in phosphate buffer can be strong evidence for this effect: the first oxidation wave of CuBor in borate buffer is 120 mV lower than the equivalent oxidation event in phosphate buffer where $[Cu(BPy)_2(ClO_4)]^+$ is mononuclear (+1.37 V according to the DPV), indicating that borate facilitates the oxidation event. To understand the significant current enhancement observed at the second oxidation wave near 1.55 V, we plotted the normalized current of this anodic wave versus the scan rate, and the plot exhibits a typical shape for an EC process (Figure S12).[20] In addition, when scanning from 0 V to +1.90 V and reversing the scan back to −0.8 V, a new reduction wave was observed at −0.28 V, which can be assigned to the reduction of dioxygen.[4a] Indeed, the CV scan of a buffer solution saturated with O_2, produced the same reduction wave at −0.28 V. Moreover, when scanning from 0 to +1.38 V (right before the onset of the second oxidation wave), and back, a different reduction wave, at −0.21 V was obtained (Figure S13). This peak at −0.21 V can be assigned to the reduction of Cu^{II} to Cu^{I} because it is also observed when a CV scan from 0 V to −0.8 V is performed under N_2. Overall, these results indicate that dioxygen is formed after the second oxidation and therefore suggest that the second irreversible reaction is the catalytic event for WO.

Oxygen evolution was explored in a solution of 0.25 mM CuBor for a 10-hour CPE experiment at applied potential +1.5 V (Figure 3, Figure S14). After 10 h, 0.15 C was accumulated and 0.2 μmol of dioxygen was evolved in the absence of the catalyst, while a charge of 4.9 C was accumulated, 11.4 μmol of dioxygen was evolved and a current of about 0.19 mA/cm^2 was measured in the presence of CuBor. Accordingly, the FE% and turnover number (TON) were calculated to be 91% and 9.5, respectively. Additionally, horseradish peroxidase (HRP) was added to the solution after CPE, following by a UV-Vis measurement which indicated that no H_2O_2 was produced during the catalytic reaction (Figure S15).[21] Notably, 0.25 mM $[Cu(BPy)_2(ClO_4)]^+$ in phosphate buffer resulted in a negligible current in the same reaction conditions, and only a small amount of dioxygen was generated (Figure S16), indicating, again, the significant role of borate buffer in this reaction.

CuBor remained intact during the entire 10-hour CPE experiment as suggested by the UV-Vis and ATR-FTIR taken after the CPE, which did not show any shift of the absorption or transmittance bands respectively (Figures S17-18). High-resolution scanning electron microscope (HR-SEM) images of the ITO working electrode before and after the 10-hour CPE experiment showed no particle deposited on the electrode surface (Figure S19). Likewise, the elemental analysis of the electrode surface, conducted by energy-dispersive X-ray spectroscopy (EDX), did not detect Cu, supporting our conclusion that no Cu-related particle is formed on the working electrode during 10-hour CPE (Figure S20). Additionally, after CPE experiment with CuBor, the ITO working electrode was used without cleaning in a subsequential CPE experiment in a fresh borate buffer solution without any catalyst. Its current response is identical to the current response of a clean ITO electrode in the same conditions (Figure S21). We, therefore, deduced that this is a homogeneous process. To further clarify it, we removed the glassy electrode from a solution of CuBor after carrying out 20 continuous CV scans (Figure S22), rinsed (but not polished) it

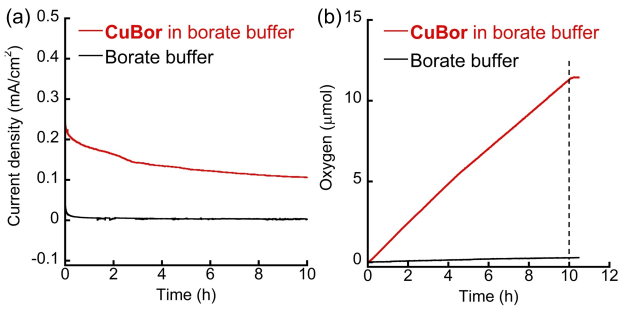

Figure 3. (a) Current density of 0.25 mM CuBor and blank in 0.2 M borate buffer at pH 9 for CPE experiments at +1.5 V; (b) corresponding accumulated oxygen; the dashed line represents the end of electrolysis. All the experiments were done using ITO (1.0 cm^2) as the working electrode and Ag/AgCl as the reference electrode.

with deionized water, and placed it in fresh 0.2 M borate buffer solution at pH 9.[22] The CV scan of this electrode showed no catalytic response and was almost identical to the CV of a clean electrode (Figure S23). Moreover, performing the CV at different scan rates showed that the i_p of the first oxidation varies linearly with $v^{1/2}$ (Figure 4a). Considering the irreversibility, i_p and $v^{1/2}$ follow the relation in Equation (1):

$$i_p = 0.446(n_pF)^{3/2}A[Cu](\alpha D_{Cu}v/RT)^{1/2} \quad (1)$$

The diffusion coefficient D_{Cu} was calculated to be 1.4×10^{-5} cm^2/s by the slope of the linear plot, which is consistent with a diffusion-controlled process, further supporting a homogeneous reaction.

Kinetic studies revealed that the current intensities of both oxidations, i_p and i_{cat}, vary linearly with the concentrations of CuBor (Figure S24).[23] This first-order kinetics suggests a single-molecular catalysis for WO, rather than polymerization or aggregation during electrolysis. Concurrently, the ratio of i_{cat} and i_p in different catalyst concentrations can be utilized to evaluate the turnover frequency (TOF) by foot-of-the-wave analysis (FOWA) by utilizing the linear slopes of i_{cat}/i_p versus 1/[1 + exp(E^0–E)F/RT] near the onset potential. The TOF calculated by FOWA is defined as TOF_0.[12][24] This analysis of CuBor afforded calculated k_{obs} (= TOF_0) values ranging between 242 to 391 s^{-1} (Eq. S7, Figure S25). Accordingly, the average TOF_0 is 310 s^{-1}, which is relatively high compared to that of other reported homogenous WOCs by the same method and might be associated with the role of the borate buffer in the catalytic process.[10]

To explore this possibility, we wished to study the mechanism of WO catalyzed by CuBor. Specifically, we wanted to understand whether the borate buffer has a role in the rate-determining step of the WO reaction. As shown in Figure S26, i_{cat} increases with the increasing borate concentration, which can provide additional evidence for the participation of borate in the catalytic process. It was previously shown that in a buffer-assisted process, the rate constant, k_{cat}, can be expressed by the sum of the rate in unbuffered solution (k_{water}) and the rate with the addition of buffer (k_B[B]), as shown in Equation (2).[25]

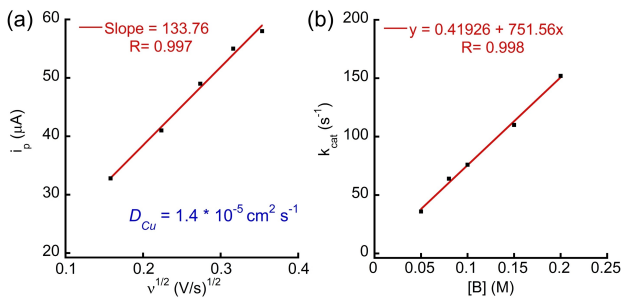

Figure 4. (a) The plot of i_p vs. $v^{1/2}$ of CuBor in 0.2 M borate buffer at pH 9.0; (b) the plot of k_{cat} vs. borate concentration [B] for catalyst CuBor; the ion strength, *I*, was maintained as 0.2 M by addition of solid KNO_3.

$$k_{cat} = k_{water} + k_B[B] \quad (2)$$

The value of $(i_{cat}/i_{water})^2$ is linearly correlated to the concentration of borate buffer, [B], which fits in Equation (3) and clearly illustrates that borate participates in the rate-determining step as first-order reaction (Figure S27):[7a,21]

$$(i_{cat}/i_{water})^2 = k_{cat}/k_{water} = 1 + k_B[B]/k_{water} \quad (3)$$

In single-molecular catalysis, i_{cat} can be defined as

$$i_{cat} = n_{cat}FA[Cu](k_{cat}D_{Cu})^{1/2} \quad (4)$$

where n_{cat} is 4 for WO, *F* is faradaic constant, A is the active surface area of working electrode, [Cu] is the catalyst concentration, and D_{Cu} is 1.4×10^{-5} cm^2/s. Therefore, the i_{cat} obtained in electrochemical WO catalyzed by CuBor in different borate buffer concentrations at pH 9 was calculated for k_{cat} according to Equation (4) and plotted versus [B] (Figure 4b). Fitting the linear correlation (as in Equation (2)), k_B was determined by this linear slope, to be 7.5×10^2 M^{-1} s^{-1} with k_{water} determined from the intercept as 0.42 s^{-1}. To the best of our knowledge, this is the first time that k_B for borate buffer is determined for WO. Moreover, this value is higher than previously reported values for other buffers (Table S2). This is quantitative evidence for the significant role of borate buffer in electrocatalytic WO.

In order to propose a mechanism for the CuBor electro catalyzed WO reaction, we considered the following findings that were discussed above, namely: (1) the WO catalyzed by CuBor is a single-molecular process, (2) CuBor undergoes two-electron oxidation prior to the rate-determining step and (3) borate participates in the rate-determining step of WO. In addition, a Pourbaix diagram, constructed from CVs in different pH units, demonstrated that the two oxidation waves resulted in slope values of 0.061 and 0.063, respectively, implying two proton-coupled-electron transfer (PCET) processes (Figure S28),[26] and possible coordination of CuBor to H_2O for proton transfer. Indeed, the CV of CuBor showed obvious inhibition in catalysis in the presence of acetonitrile, a potential competitor for this coordination (Figure S24), supporting water coordination as an initial step in the reaction. Taking all the above findings into account, we can suggest that in the first step of the reaction, CuBor coordinates to H_2O ([CuBor-H_2O]$^{3+}$) and then undergoes a $2H^+/2e^-$ PCET process, in which either [CuBor–O$^\bullet$]$^{3+}$ or [CuBor=O]$^{3+}$ are formed (Step 1, Figure S27).[27] Another CPE experiment at +1.25 V showed that only a small amount of oxygen was generated but the formation of H_2O_2 as $2H^+/2e^-$ process from water was excluded by UV-Vis measurements with HRP (Figure S29). Therefore, it is reasonable that the key intermediate ([CuBor–O$^\bullet$]$^{3+}$ or [CuBor=O]$^{3+}$) is formed after the first oxidation. However, the rate-determining step and later PCET process are largely contributed by the second oxidation, which is more significant for the fast kinetic WO.[25b,28] In the rate-determining step, this intermediate can undergo either an intermolecular two metal-oxo coupling (I2 M) or a nucleophilic attack, typically by water (WNA) towards

O–O bond formation.[3d,29] To probe this point we have calculated k_{obs} by FOWA and found that it is concentration-independent (Figure S25b). Hence, we could eliminate the I2 M pathway for O–O bond formation. We therefore propose that a nucleophilic attack mechanism is taking place, and suggest that instead of the typical WNA, oxygen is transferred from water via $B(OH)_4^-$, which is a known oxygen-donor.[5c,10] The involvement of borate species in the rate-determining step is also supported by the high k_B as discussed above. We also conducted a kinetic isotope effect (KIE) study using H_2O vs. D_2O, and calculated that the KIE value is 1.1 (Figure S30), revealing that the atom-proton transfer (APT) process does not occur during O–O bond formation.[24,30] Taking these results together, we suggest that the O–O bond formation is enabled through an intermolecular $B(OH)_4^-$-anion-nucleophilic attack pathway, instead of I2 M or WNA, leading to the formation of $[CuBor–OOH]^{2+}$ (Step 2, Figure S31). Finally, we suggest that the additional PCET process ($1H^+/1e^-$) and one-electron transfer taking part in the last stage of the reaction occur, leading to the release of dioxygen and regeneration of $[CuBor\text{-}H_2O]^{3+}$ (Step 3, Figure S27).

Conclusion

In this work we disclose a unique tri-copper borate complex, CuBor, that is composed of inexpensive and readily available precursors, as an active electrocatalyst for homogeneous WO, through a nucleophilic attack mechanism, and show that the borate buffer plays both a structural and a functional role in the catalysis. The understanding gained from this study should lead to the development of WO systems that consider the buffer solution in the catalyst design. To this end, our study demonstrates the use of borate buffer for the construction of low-cost and easily synthesized WO electrocatalyst as a promising approach for the future development of WO catalysts.

Experimental Section

Synthesis of $[Cu(BPy)_2(ClO_4)](ClO_4)$: Following the literature,[11] 2,2′-bipyridine (0.16 g, 1.0 mmol) dissolved in 30 mL of acetonitrile was added dropwise to a solution of copper(II) perchlorate hexahydrate $[Cu(ClO_4)_2.6H_2O]$ (0.19 g, 0.5 mmol) in 20 mL of acetonitrile with constant stirring under air for 1 h. The blue precipitate was filtered and washed with acetonitrile and ether 3 times, dried and recrystallized in water affording needle-like blue crystals suitable for X-ray analysis (CCDC number 2145498). Elemental analysis calc (%) for $C_{20}H_{16}Cl_2CuN_4O_8$: C 41.79, H 2.81, N 9.75; found: C 41.61, H 2.75, N 9.64.

Synthesis of CuBor and CuAce: $[Cu(BPy)_2(ClO_4)](ClO_4)$ was dissolved in 0.2 M borate or acetate buffer at pH 9.0, and the solution was left undisturbed under open air environment. Within 3 weeks, rectangular-shaped or needle-shaped blue crystals were obtained, collected, and analyzed (CCDC numbers 2145497 and 2171820). Elemental analysis calc (%) for $C_{60}H_{48}BCl_4Cu_3N_{12}O_{19}$: C 45.46, H 3.03, N 10.61; found: C 44.38, H 2.98, N 9.97. The crystal structure of CuAce was previously reported in the literature.[18]

Electrochemical Methods: Cyclic voltammetry (CV), and differential pulse voltammetry (DPV) experiments were carried out on an EmStat3 potentiosta tusing one-compartment three-electrode cells, Glassy Carbon (GC) as the working electrode, Ag/AgCl as the reference electrode, and Pt wire as the counter electrode. All redox potentials are reported versus Ag/AgCl. CVs were collected at 100 mV/s except for other specifications. DPV was obtained with the following parameters: Amplitude = 200 mV, E-step = 10 mV, pulse width = 0.02 s.

Oxygen Evolution Experiment: Controlled potential electrolysis (CPE) experiments were performed using a sealed two-compartment cell, porous carbon as working electrode and Ag/AgCl as reference electrode and a mesh platinum counter electrode was used. The solution was purged with nitrogen gas prior to each measurement. Oxygen evolution was monitored in the gas phase with a fixed needle-type oxygen minisensor (from PyroScience) placed in the headspace of the reaction vassal (working electrode side). During the CPE experiments solutions of both compartments were vigorously stirred. The Faraday efficiency was determined according to the total charge passed during the CPE and the total amount of generated oxygen as a four-electron oxidation process. The oxygen was measured by the oxygen sensor in % and converted to μmol using a calibration curve (for more details see Supporting Information).

Deposition Numbers 22145497 (for CuBor), 2145498 (for $[Cu(BPy)_2(ClO_4)](ClO_4)$), and 2171820 (for CuAce) contain the supplementary crystallographic data for this paper. These data are provided free of charge by the joint Cambridge Crystallographic Data Centre and Fachinformationszentrum Karlsruhe Access Structures service.

Acknowledgements

The authors thank Prof. Yeshayahu Talmon and Mrs. Asia Matatyaho-Yaakobi from the Wolfson Department of Chemical Engineering for HR-SEM and EDX measurements and analysis. The authors also thank Dr. Rachel Edrei from the Schulich Faculty of Chemistry for elemental analysis, and Dr. Boris Tumansky from the Schulich Faculty of Chemistry for EPR measurements.

Conflict of Interest

The authors declare no conflict of interest.

Data Availability Statement

The data that support the findings of this study are available in the supplementary material of this article.

Keywords: borate buffer · copper · electrocatalysis · trinuclear · water oxidation

[1] L. Schlapbach, A. Zuttel, *Nature* **2001**, *414*, 353–358.
[2] a) J. P. McEvoy, G. W. Brudvig, *Chem. Rev.* **2006**, *106*, 4455–4483; b) J. D. Blakemore, R. H. Crabtree, G. W. Brudvig, *Chem. Rev.* **2015**, *115*, 12974–13005.

[3] a) M. N. Kushner-Lenhoff, J. D. Blakemore, N. D. Schley, R. H. Crabtree, G. W. Brudvig, *Dalton Trans.* **2013**, *42*, 3617–3622; b) B. Das, A. Rahaman, A. Shatskiy, O. Verho, M. D. Karkas, B. Akermark, *Acc. Chem. Res.* **2021**, *54*, 3326–3337; c) J. Lloret-Fillol, M. Costas, *Adv. Organomet. Chem.* **2019**, *71*, 1–52; d) X. Sala, S. Maji, R. Bofill, J. Garcia-Anton, L. Escriche, A. Llobet, *Acc. Chem. Res.* **2014**, *47*, 504–516.
[4] a) S. M. Barnett, K. I. Goldberg, J. M. Mayer, *Nat. Chem.* **2012**, *4*, 498–502; b) T. Ghosh, P. Ghosh, G. Maayan, *ACS Catal.* **2018**, *8*, 10631–10640; c) Q. Y. Mao, Y. J. Pang, X. C. Li, G. J. Chen, H. W. Tan, *ACS Catal.* **2019**, *9*, 8798–8809; d) D. L. Gerlach, S. Bhagan, A. A. Cruce, D. B. Burks, I. Nieto, H. T. Truong, S. P. Kelley, C. J. Herbst-Gervasoni, K. L. Jernigan, M. K. Bowman, S. Pan, M. Zeller, E. T. Papish, *Inorg. Chem.* **2014**, *53*, 12689–12698; e) T. Zhang, C. Wang, S. Liu, J. L. Wang, W. Lin, *J. Am. Chem. Soc.* **2014**, *136*, 273–281; f) T. T. Li, Y. Q. Zheng, *Dalton Trans.* **2016**, *45*, 12685–12690; g) M. Gil-Sepulcre, P. Garrido-Barros, J. Oldengott, I. Funes-Ardoiz, R. Bofill, X. Sala, J. Benet-Buchholz, A. Llobet, *Angew. Chem. Int. Ed.* **2021**, *60*, 18639–18644; h) V. K. K. Praneeth, M. Kondo, P. M. Woi, M. Okamura, S. Masaoka, *ChemPlusChem* **2016**, *81*, 1123–1128.
[5] a) Z. Chen, T. J. Meyer, *Angew. Chem. Int. Ed. Engl.* **2013**, *52*, 700–703; b) S. G. Winikoff, C. J. Cramer, *Catal. Sci. Technol.* **2014**, *4*, 4099–4099; c) H. H. Huang, J. W. Wang, P. Sahoo, D. C. Zhong, T. B. Lu, *Chem. Commun.* **2017**, *53*, 9324–9327.
[6] H. Lee, X. Wu, L. Sun, *Nanoscale* **2020**, *12*, 4187–4218.
[7] a) M. K. Coggins, M. T. Zhang, Z. Chen, N. Song, T. J. Meyer, *Angew. Chem. Int. Ed. Engl.* **2014**, *53*, 12226–12230; b) J. W. Wang, X. Q. Zhang, H. H. Huang, T. B. Lu, *ChemCatChem* **2016**, *8*, 3287–3293; c) D. Wang, J. T. Groves, *Proc. Natl. Acad. Sci. USA* **2013**, *110*, 15579–15584.
[8] M. W. Kanan, D. G. Nocera, *Science* **2008**, *321*, 1072–1075.
[9] a) M. Dinca, Y. Surendranath, D. G. Nocera, *Proc. Natl. Acad. Sci. USA* **2010**, *107*, 10337–10341; b) F. S. Yu, F. Li, B. B. Zhang, H. Li, L. C. Sun, *ACS Catal.* **2015**, *5*, 627–630; c) Q. F. Chen, H. Y. Du, M. T. Zhang, *Chin. J. Catal.* **2021**, *42*, 1338–1344.
[10] G. L. Ruan, P. Ghosh, N. Fridman, G. Maayan, *J. Am. Chem. Soc.* **2021**, *143*, 10614–10623.
[11] E. Garribba, G. Micera, D. Sanna, L. Strinna-Erre, *Inorg. Chim. Acta* **2000**, *299*, 253–261.
[12] a) C. Costentin, S. Drouet, M. Robert, J. M. Saveant, *J. Am. Chem. Soc.* **2012**, *134*, 11235–11242; b) C. Costentin, J.-M. Savéant, *ChemElectroChem* **2014**, *1*, 1226–1236; c) R. Matheu, S. Neudeck, F. Meyer, X. Sala, A. Llobet, *ChemSusChem* **2016**, *9*, 3361–3369.
[13] T. Ghosh, N. Fridman, M. Kosa, G. Maayan, *Angew. Chem. Int. Ed. Engl.* **2018**, *57*, 7703–7708.
[14] J. Schott, J. Kretzschmar, M. Acker, S. Eidner, M. U. Kumke, B. Drobot, A. Barkleit, S. Taut, V. Brendler, T. Stumpf, *Dalton Trans.* **2014**, *43*, 11516–11528.
[15] a) M. Okeeffe, N. E. Brese, *J. Am. Chem. Soc.* **1991**, *113*, 3226–3229; b) I. D. Brown, *Chem. Rev.* **2009**, *109*, 6858–6919.
[16] a) N. Gluz, G. Christou, G. Maayan, *Chem. Eur. J.* **2021**, *27*, 6034–6043; b) N. Wannarit, N. Chaichit, C. Pakawatchai, S. Youngme, *Russ. J. Coord. Chem.* **2010**, *36*, 778–785.
[17] a) P. P. Y. Chen, R. B. G. Yang, J. C. M. Lee, S. I. Chan, *Proc. Natl. Acad. Sci. USA* **2007**, *104*, 14570–14575; b) E. A. Malinina, I. K. Kochneva, I. N. Polyakova, V. V. Avdeeva, G. A. Buzanov, N. N. Efimov, E. A. Ugolkova, V. V. Minin, N. T. Kuznetsov, *Inorg. Chim. Acta* **2018**, *479*, 249–253.
[18] B. J. Hathaway, N. Ray, D. Kennedy, N. Obrien, B. Murphy, *Acta Crystallogr. Sect. B* **1980**, *36*, 1371–1377.
[19] a) E. Laviron, *J. Electroanal. Chem.* **1979**, *101*, 19–28; b) X. Jiang, J. Li, B. Yang, X. Z. Wei, B. W. Dong, Y. Kao, M. Y. Huang, C. H. Tung, L. Z. Wu, *Angew. Chem. Int. Ed.* **2018**, *57*, 7850–7854; *Angew. Chem.* **2018**, *130*, 7976–7980.
[20] H. M. Shahadat, H. A. Younus, N. Ahmad, S. G. Zhang, S. Zhuiykov, F. Verpoort, *Chem. Commun.* **2020**, *56*, 1968–1971.
[21] a) H. Li, F. Xie, M. T. Zhang, *ACS Catal.* **2021**, *11*, 68–73; b) V. Sanz, S. de Marcos, J. R. Castillo, J. Galban, *J. Am. Chem. Soc.* **2005**, *127*, 1038–1048.
[22] D. J. Wasylenko, R. D. Palmer, E. Schott, C. P. Berlinguette, *Chem. Commun.* **2012**, *48*, 2107–2109.
[23] M. C. Kafentzi, R. Papadakis, F. Gennarini, A. Kochem, O. Iranzo, Y. Le Mest, N. Le Poul, T. Tron, B. Faure, A. J. Simaan, M. Reglier, *Chem. Eur. J.* **2018**, *24*, 5213–5224.
[24] F. Chen, Z. Y. Cheng, R. Z. Liao, M. T. Zhang, *J. Am. Chem. Soc.* **2021**, *143*, 19761–19768.
[25] a) Z. F. Chen, J. J. Concepcion, X. Q. Hu, W. T. Yang, P. G. Hoertz, T. J. Meyer, *Proc. Natl. Acad. Sci. USA* **2010**, *107*, 7225–7229; b) Y. Tamaki, A. K. Vannucci, C. J. Dares, R. A. Binstead, T. J. Meyer, *J. Am. Chem. Soc.* **2014**, *136*, 6854–6857.
[26] D. R. Weinberg, C. J. Gagliardi, J. F. Hull, C. F. Murphy, C. A. Kent, B. C. Westlake, A. Paul, D. H. Ess, D. G. McCafferty, T. J. Meyer, *Chem. Rev.* **2012**, *112*, 4016–4093.
[27] a) M. T. Zhang, Z. F. Chen, P. Kang, T. J. Meyer, *J. Am. Chem. Soc.* **2013**, *135*, 2048–2051; b) I. Funes-Ardoiz, P. Garrido-Barros, A. Llobet, F. Maseras, *ACS Catal.* **2017**, *7*, 1712–1719.
[28] M. K. Coggins, M. T. Zhang, Z. F. Chen, N. Song, T. J. Meyer, *Angew. Chem. Int. Ed.* **2014**, *53*, 12226–12230; *Angew. Chem.* **2014**, *126*, 12422–12426.
[29] J. W. Wang, W. J. Liu, D. C. Zhong, T. B. Lu, *Coord. Chem. Rev.* **2019**, *378*, 237–261.
[30] X. J. Su, M. Gao, L. Jiao, R. Z. Liao, P. E. M. Siegbahn, J. P. Cheng, M. T. Zhang, *Angew. Chem. Int. Ed.* **2015**, *54*, 4909–4914; *Angew. Chem.* **2015**, *127*, 4991–4996.

Manuscript received: August 2, 2022
Accepted manuscript online: August 30, 2022
Version of record online: September 26, 2022